CrossMark

Effect of Na doping on structure, morphology and properties of hydrothermally grown one dimensional TiO$_2$ nanorod structures

S. Shalini[1] · N. Prabavathy[1] · R. Balasundaraprabhu[1] · T. Satish Kumar[2] ·
Pravin Walke[3] · S. Prasanna[4] · Dhayalan Velayuthapillai[5]

Abstract Na doped TiO$_2$ nanorod structures have been prepared by one-step hydrothermal method. Structural analysis of undoped and doped TiO$_2$ nanorod samples revealed the formation of single rutile phase structure. XRD plots confirms the effective substitution of Ti^{4+} with Na$^+$ in the samples by exhibiting a slight shift towards the lower angle in the 2θ value of the diffraction peaks compared to undoped TiO$_2$ sample. The distribution of sodium in TiO$_2$ lattice is confirmed by morphological and EDS analysis. FESEM images of doped samples revealed the formation of structures in the form of nanorods for 2 and 4% of dopant and then to nanoflowers on increasing the amount of dopant to 6%. TEM analysis revealed the formation of nanorods with a diameter about 250 nm. Each nanorod was found to be formed of individual thin nanorods with approx diameter of 25 nm. The presence of sodium (atomic% = 7.60) in the nanorods was also substantiated by EDS studies. From optical studies, with increase in dopant concentration, the absorption edge is

seen to be shifted towards the longer wavelength and bandgap tends to show red shift with values varying from 3.0 to 2.74 eV.

1 Introduction

Recently, one dimensional (1D) nanomaterials such as nanorods, nanowires, nanotubes etc. have attracted considerable attraction due to their interesting properties and wide spread applications. Enhanced electron transport and quick separation of photo-generated electrons and holes along opposite direction to retard the recombination of electron–hole pairs make these 1D structures suitable candidates for applications in the areas of solar photovoltaics and several other optoelectronic devices [1, 2]. Among the 1D nanomaterials like TiO$_2$, ZnO, SnO$_2$, NiO and V$_2$O$_5$, titanium dioxide (TiO$_2$) with wide bandgap of 3.0 eV is chosen as a candidate of study due to its advantages like long lifetime of excited electrons, suitable band edge levels for charge injection and extraction, chemical stability, non-toxicity, natural abundance and low cost [3]. Apart from the advantages listed above, TiO$_2$ is also a very suitable oxide material as a photoanode in dye-sensitized solar cells (DSSC) due of its extraordinary ability to oxidize photogenerated holes [4]. In addition to their physical and chemical properties, the geometries of TiO$_2$ nanostructures plays a vital role in determining the performances of DSSCs. TiO$_2$ can be synthesized in variety of forms such as rods, tubes, sheets, and wires by sol–gel [5], solvothermal [6] and hydrothermal methods [7]. Hydrothermal method is widely chosen as it is a one-step method involving low operating temperatures and less growth time.

S. Prasanna on leave from PSG CT, Coimbatore, India.

✉ S. Shalini
  shalini1689@gmail.com

1   Centre for sustainable photovoltaic technology, Department of Physics, PSG College of Technology, Coimbatore, Tamil Nadu 641004, India

2   Department of Metallurgical Engineering, PSG College of Technology, Coimbatore, Tamil Nadu 641004, India

3   Centre for Nanosciences and Nanotechnology, University of Mumbai, Vidyanagari, Kalina, Santacruz (East), Mumbai 400098, India

4   Department of Physics, University of Idaho, Moscow, USA

5   Department of Engineering, University College of Bergen, Bergen, Norway

Among the different 1D structures, nanorods are chosen for the present work as TiO_2 nanorods provides a large surface area for dye loading and in turn reduces the electron loss during the transfer of photo generated electrons [8]. Doping of TiO_2 with metal or nonmetal atoms is an effective way to extend the absorption of TiO_2 from UV to visible region as visible-light driven 1D TiO_2 nanomaterials are highly desired [9]. Doping can also easily shift the band edge and Fermi level of the material and thus change the electron transfer properties [10]. Doping of TiO_2 is more complicated because of the defect ridden state of TiO_2 and doping affects the trap states and electronic structure of TiO_2 [11]. When TiO_2 is doped with metallic or non metallic ions, either the cation Ti^{4+} can be affected or the anion O^{2-} can be affected. As the lower edge of conduction band is comprised of Ti^{4+} 3d bands, doping of Ti^{4+} is found to have a profound effect on the properties of TiO_2 as the dopant can induce oxygen vacancies [12]. Dye absorption and superior charge transport efficiency can be significantly improved by doping [12].

Liu et al. [13] on doping TiO_2 with Zn^{2+} reported a positively shifted Fermi level and reduced electron–hole recombination, with improved electron densities and transport. Interstitial incorporation of Y^{3+} into the lattice of TiO_2 led to increase in surface area, increasing the dye adsorption. The optical properties were reported to be significantly modified with a decrease in bandgap and increase in conductivity [14]. Chen et al. [15] studied the effects of doping B^{3+} into TiO_2. Interstitial doping of B^{3+} led to a blue shift of the UV–Vis absorption spectrum and also led to an increase in oxygen vacancies.

There are several dopants including alkali metals, metalloids, non-metals and transition metals that are used to dope TiO_2. But to the best of authors knowledge there is only limited literature available for Na doped TiO_2 [16]. Hence in this study, an attempt has been made to synthesize Na doped TiO_2 nanorods with different amount of sodium by one-step hydrothermal method. The effect of sodium on structure, morphology and optical properties has been investigated.

2 Need for doping alkali metals and choice of Na as dopant

In the case of alkali metals, the outer electron shell of these metals consists of 's' electrons which can be easily donated, thereby making these metals interesting cationic dopants for TiO_2. Commonly employed alkali metals for doping TiO_2 are lithium [17] and sodium [16]. Doping of lithium and unintentional adsorption of Li^+ ions from the electrolyte (iodide tri iodide redox couple in DSSC) to TiO_2, results in a positive shift of the CB and reduced recombination rate [18].

Doping of sodium is believed to serve two purpose, as Na^+ ions when doped into TiO_2 modifies the morphology and optical properties by exciting the absorption of TiO_2 from UV to visible region. As a next step, it acts as a mordant. Mordants are water soluble substances that partly or wholly combine with natural dye molecule by forming covalent and coordination bonds. It is believed that mordants are capable of fixing and improving the dye absorption by the film. The most important class of mordants include tannic acid, alum, sodium chloride, and certain salts of aluminium, chromium, copper, iron, iodine, potassium, sodium, and tin. These mordants serve for the fixation of acid or phenol-like natural dyes [19]. It has been observed that most of the mordants are toxic in nature. Among all the mordants, sodium chloride is chosen as it is non-hazardous, easily available, cheap and is a neutral catalyst that helps to speed up the dye uptake by the film.

3 Materials and methods

3.1 Materials

FTO (fluorine doped tin oxide) of sheet resistance 7 $\Omega/\square$ was used as substrate. Titanium isopropoxide ($Ti[OCH(CH_3)2]4$, 97% purity) and Hydrochloric acid (HCl, 98% purity), Sodium Chloride (NaCl, 98% purity) were used as precursors to synthesis of TiO_2 nanorods and doped TiO_2 nanorods. All the materials used in this study were purchased from Sigma-Aldrich and used without any further purification.

3.2 Method

This study involves synthesis of TiO_2 nanorods and Na-doped TiO_2 nanorods by hydrothermal method.

3.2.1 Synthesis of TiO_2 nanorods by hydrothermal method

FTO substrates were cleaned ultrasonically using soap solution, distilled water, acetone and ethanol for 10 min and dried. For preparation of TiO_2 nanorods by hydrothermal method, required quantity of HCl and deionized water was mixed and stirred for 10 min. Then $Ti[OCH(CH_3)_2]_4$ was added to the stirring mixture as droplets. The mixture was again stirred for another 10 min to achieve homogeneity, and transferred into Teflon-lined stainless steel autoclave (50 ml) with substrates pre-loaded into it. Then the autoclave was sealed and hydrothermally treated in a muffle furnace at 170 °C for 4 h. After cooling down to room temperature, the samples were washed with deionized water several times and dried at room temperature overnight.

3.2.2 Synthesis of Na-doped TiO_2 nanorods by hydrothermal method

Typically, required quantity of HCl and deionized water was mixed and stirred for 10 min. Then $Ti[OCH(CH_3)_2]_4$ was added to the stirring mixture as droplets and stirred again for 10 min. Finally, to synthesize Na doped TiO_2 nanorods, different perentage of NaOH (2, 4 and 6%) was dissolved with required amount of distilled water and added to the stirring mixture. The mixture was stirred for another 30 min to achieve homogeneity, and transferred into Teflon-lined stainless steel autoclave (50 ml) with substrates pre-loaded into it. Then the autoclave sealed and hydrothermally treated in a muffle furnace at 170 °C for 4 h. At the end of growth time, the autoclave was cooled down to room temperature and the samples were washed with deionized water several times and dried at room temperature overnight.

3.3 Characterization techniques

The crystalline phase of undoped and Na doped titania electrodes were analyzed using X-ray diffractometer (XRD, SHIMADZU LabX-6000) with a Cu target ($\lambda = 1.5409$ Å). A scan speed of 2°/min with the step scan of 0.02° was used with 40 kV potential. The samples were scanned with 2θ values ranging from 10° to 80°. The angles of the characteristic peaks were measured from the plot and indexed by using PCPDF data. The shape and size of the synthesized nanorods were analyzed using field emission scanning electron microscopy (FE-SEM, ZEISS, SIGMA, UK) and high-resolution transmission electron microscopy (HR-TEM, JEOL, JEM 2100) equipped with energy dispersive spectroscopy (EDS). Absorbance of the films and the information about band gap energy of Na doped nanorod films were recorded using a Jasco UV–Vis-DRS (Model V570) spectrometer operating at a resolution of 2 nm.

4 Results and discussion

4.1 Structural analysis

In order to confirm the crystalline phase of undoped and Na-doped TiO_2 nanorods, XRD study was carried out. Figure 1 shows the XRD plot of undoped and Na doped TiO_2 nanorods. From the plot it is clearly seen that all the peaks (2θ positions of 27.39°, 36.08°, 39.10°, 41.3°, 43.97°, 54.36° and 56.68°) corresponds only to the rutile phase TiO_2 (JCPDS No. 890555). Moreover, rutile TiO_2 has a verysmall lattice mismatch (<2%) with FTO and is easy to grow on FTO with large aspect ratio [20]. No extra
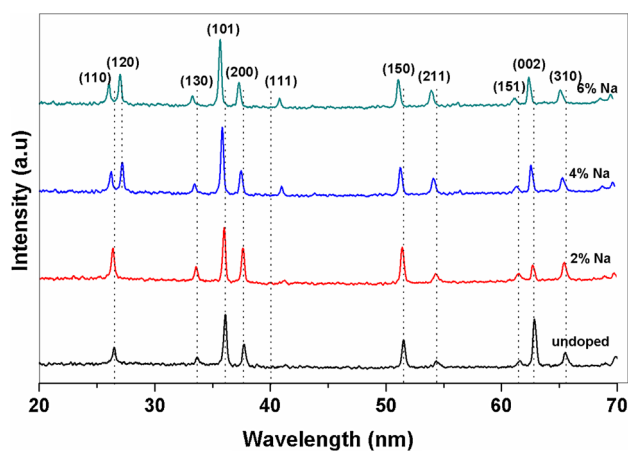
Fig. 1 XRD pattern of undoped and 2, 4 and 6% doped TiO_2 nanorod

peaks corresponding to other phases of TiO_2 such as anatase or brookite was observed.

The observed pattern of Na-doped samples reveal strong peaks corresponding to pure rutile phase as observed in the case of undoped TiO_2 nanorod sample. This doped films also exhibit perfect, single rutile phase with no impurity/additional phases. From the plot it can be clearly seen that the increase in dopant concentration led to a slight shift towards the lower angle in the 2θ value of the diffraction peaks when compared to the plot of undoped TiO_2 sample. The shift of the peaks toward lower 2θ values indicates an expansion of TiO_2 lattice and also confirms the effective substitution of Ti^{4+} with Na^+ in the samples. This is due to the difference in ionic radius of the dopant ion ($Na^+ = 1.0$ Å) and the parent ion ($Ti^{4+} = 0.61$ Å). As the radius of dopant ions is larger than the parent ion, substitution of Ti^{4+} with Na^+ will lead to induce stresses in the lattice leading to expansion of the lattice; shifting the XRD peaks toward lower 2θ values. Similar results have been reported by Li et al. [21] on doping Ti^{4+} ions with Ca^{2+} ions (ionic radius = 0.99 Å).

4.2 Morphological analysis

4.2.1 Field emission scanning electron microscopy (FESEM) studies

The surface morphology of undoped and Na-doped TiO_2 nanorods grown on FTO substrates was examined by FESEM. Figure 2a, b shows the top view FESEM pictures of undoped TiO_2 nanorods. The images reveal well-aligned, densely packed and uniform nanorods, of average length and diameter of 2 µm and 220 nm indicating that the nanorods are oriented predominantly vertical to the FTO substrates and is also consistent with the XRD result. It is also clear that the top surface of the nanorods are quite rough and the side walls are relatively smooth. The top
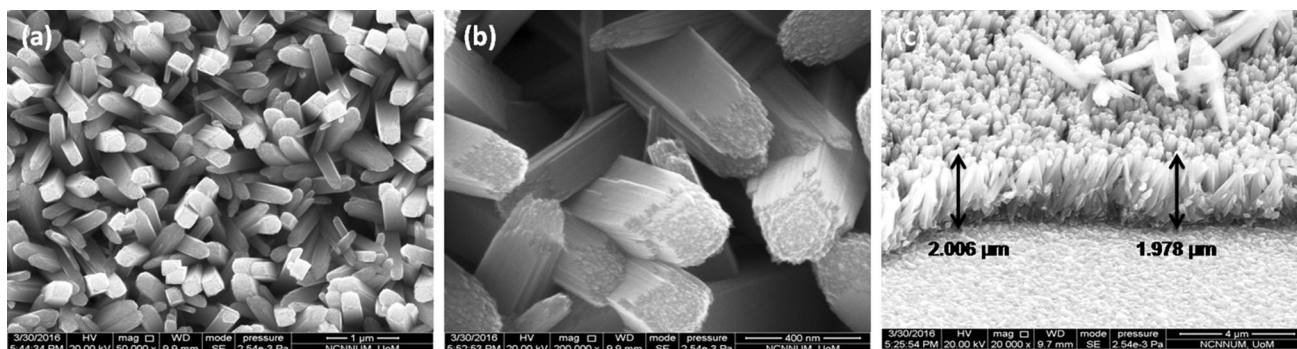
Fig. 2 **a**, **b** FESEM images of undoped TiO_2 nanorod. **c** Cross section view of undoped TiO_2 nanorod

surface of the nanorods are also of square shaped that can support the expected growth of tetragonal crystal.

Figure 3a–f shows the FESEM images of 2, 4 and 6% Na doped TiO_2 nanorods grown on FTO substrates. From Fig. 3a–d, it can be clearly seen that the surface morphology did not change significantly with 2 and 4% of Na doping. However, the length of nanorods increased on increasing the dopant concentration. The length of the nanorods as determined from FESEM images was found be respectively 2.262 and 2.309 μm for 2 and 4% of Na dopant concentration possessing an average diameter of about 250 nm. The dots seen in the FESEM images of nanorods (irrespective of dopant concentrations) reveals the presence of Na in the doped samples. This is also well substantiated by shift of peak in XRD and also from the EDS spectra. Figure 4 shows the cross section images of 2, 4 and 6% Na doped TiO_2 nanorods with length of the nanorods are marked in the FESEM image.

In the case of 6% Na doped nanorods (Fig. 3e, f), the length and average diameter of the nanorods was determined to be 2.713 and 300 nm. In this case, Na doping is found to have an obvious effect on the morphology, length and diameter of the TiO_2 nanorods. Moreover, the compactness of the nanorods were found to decrease with increase in dopant concentration. It can be understood that, increasing the dopant concentration in the growth solution decreases the nucleation density of the seed layer slowly thus reducing the compactness between the rods. From the image, it is clearly seen that concentration of Na (6%) have led to an overgrowth forming nanoflowers on the surface of the TiO_2 nanorods as the growth time and temperature are same for synthesis of all doped samples. This kind of nanoflowers on the top of nanorods is dense and uniform covering the whole surface of the substrate. The advantage of such flowers is to increase the scattering of incident light for better light harvesting. Such TiO_2 nanorod flowers are believed to provide a large surface area for higher absorption of incident photons that can lead to more photogenerated electron–hole pair. This increase in electron–hole pair can be beneficial for improvement in efficiency [22].

Studying the possible growth kinetics can pave a way to find the formation of TiO_2 nanorods leading to flower shaped overgrowth of Na–TiO_2 nanorods. The reason could be well understood by considering the increase in dopant concentration. The nanorods starts to aggregate one after the another leading to radial growth of nanorods accompanied with increase in the average diameter and length of the nanorods. Then the TiO_2 nanorods starts to aggregate and connect with one root leading to formation of 3D nanoflowers on the surface of TiO_2 nanorods.

4.2.2 Reaction of precursors and growth kinetics

1. Addition of HCl into growth solution adjusts the pH of the solution and helps to retard the hydrolysis of the precursor in the presence of water at low growth temperatures (hydrothermal growth) [22, 23].
2. When Titanium isopropoxide is added as a precursor to this acid medium, it gets hydrolyzed to titanium hydroxide and alcohol. The formed titanium hydroxide then forms a complex with water and the chemical reactions involved in the formation of TiO_2 are,

$$Ti(OR)_4 + 4H_2O \rightarrow Ti(OH)_2 + 4ROH \, (hyrolysis)$$
$$Ti(OH)_2 \rightarrow TiO_2 x H_2O + (2-x)H_2O \, (condensation)$$

3. The Cl^- ion in the growth solution restricts the growth of rutile TiO_2 in the (110) direction and promotes the growth along the (001) direction. Therefore, the growth rate of nanorod along (110) direction becomes much slower than (001) direction, leading to preferential growth of c-elongated nanorods with (110) faces. This is also confirmed by HRTEM images of TiO_2 nanorods.
4. Considering the crystal-symmetry and surface-energy of rutile TiO_2, the formed TiO_2 nanorods will exhibit a surface with square cross section and four sidewalls with (110) faces.
5. Now, when sufficient amount of dopant (NaCl) is added to the growth solution, Na^{2+} ions combine with
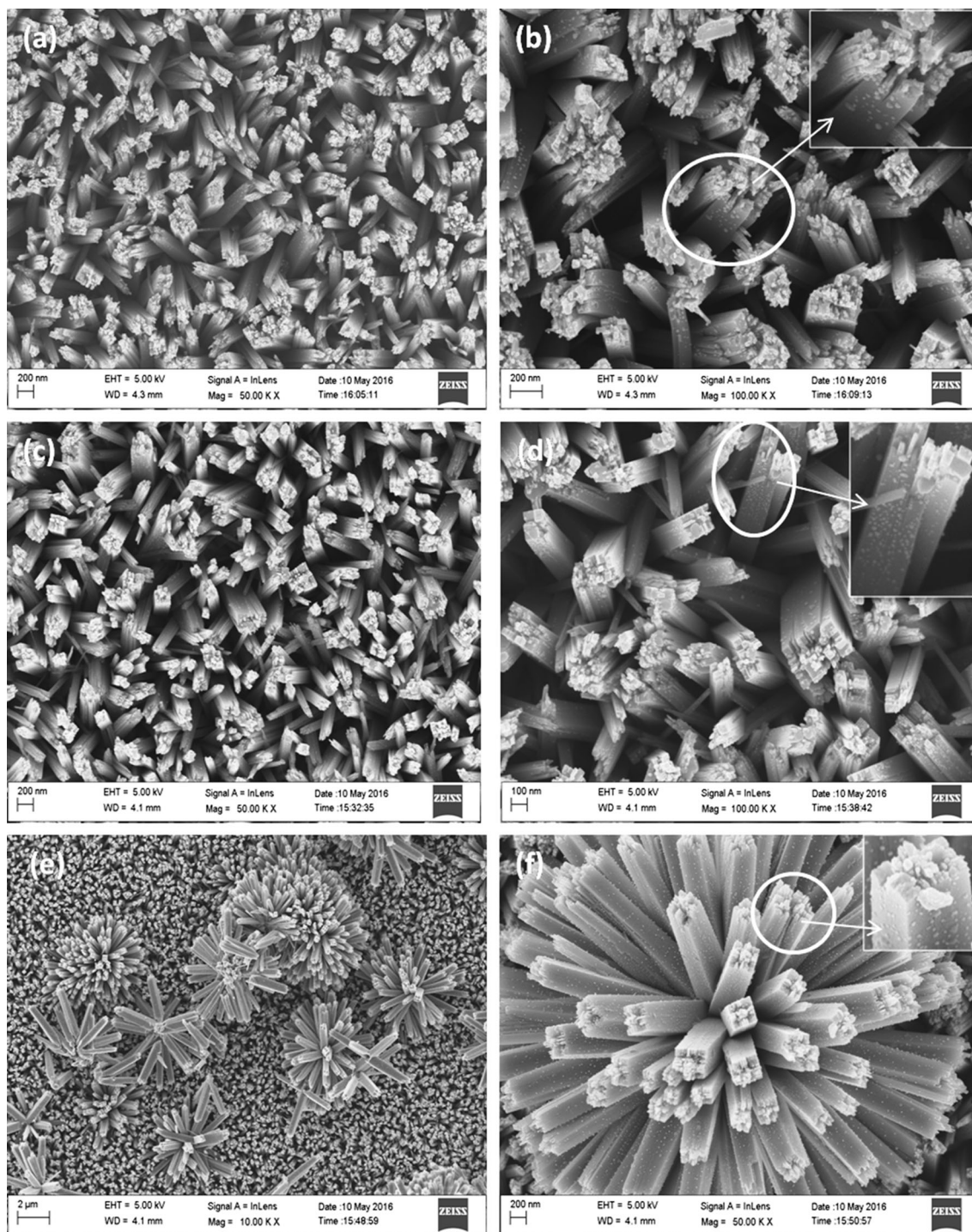
Fig. 3 FESEM images of **a**, **b** 2%, **c**, **d** 4%, **e**, **f** 6% Na doped TiO$_2$ nanorod. *Inset* in each figure shows the magnified view of a nanorod showing the presence of Na doping in the sample

OH$^-$ group to form NaOH and then forms sodium complexes in the growth solution.

6. This sodium complexes cannot act as new nucleation centers for TiO$_2$ to grow due to its surface energy conditions. As mentioned in the Sect. 4.2.1, nanorods starts to aggregate and connect with one root leading to formation of 3D nanoflowers on the surface of TiO$_2$ nanorods with increase in dopant concentration.

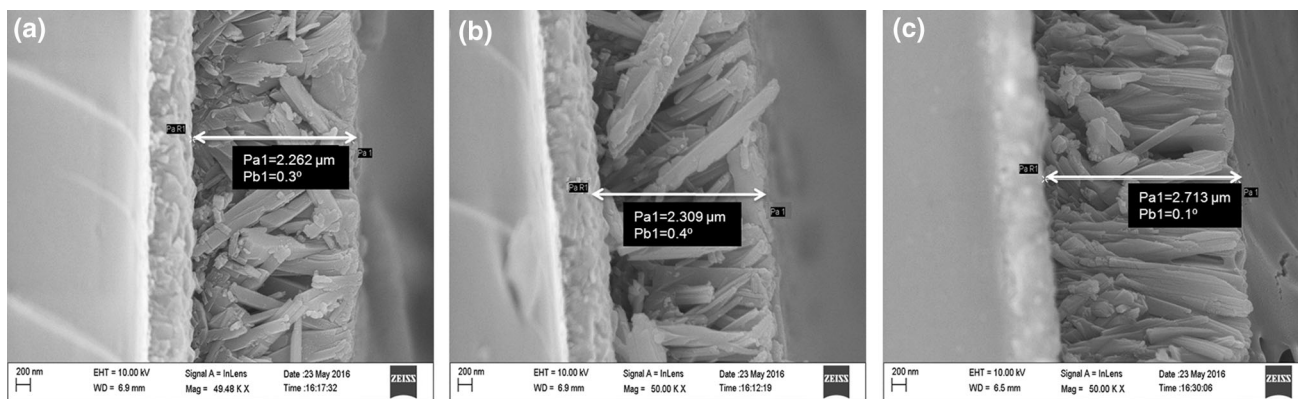Figure 5 schematically represents the growth mechanism and formation of nanorods and nanoflowers.

Fig. 4 Cross section FESEM images of 2, 4 and 6% Na doped TiO$_2$ nanorods with length of the nanorods marked in the image
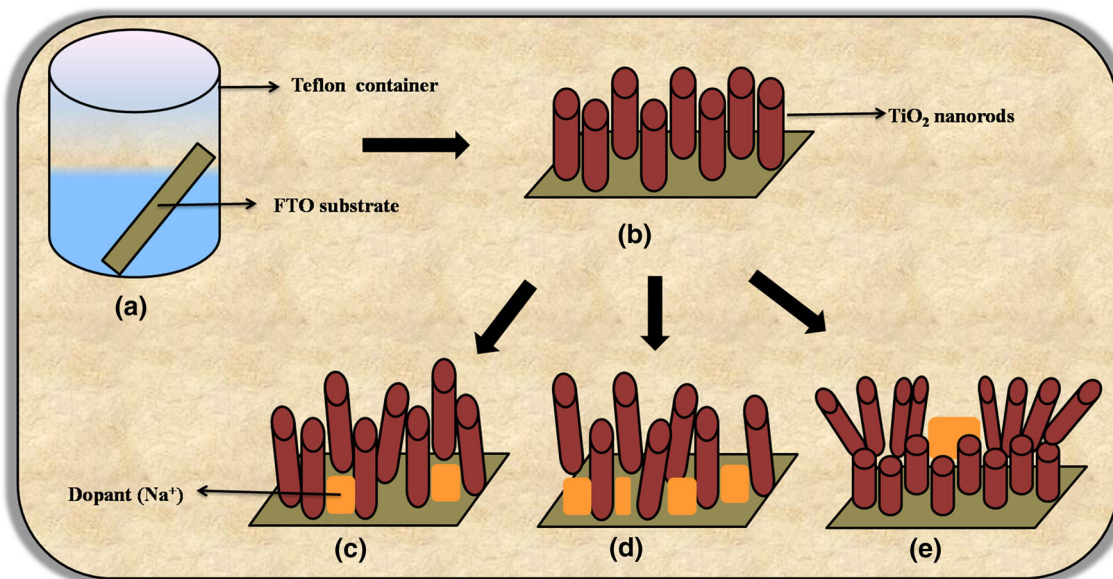

Fig. 5 Schematic representation of growth kinetics and formation of nanorods and nanoflowers

4.2.3 High resolution transmission electron microscopy (HRTEM) studies

In order to further study the formation, structure and crystallinity of TiO$_2$ nanorods, TEM analysis was carried out on undoped and doped TiO$_2$ nanorods. Figure 6a–c shows the HRTEM images of undoped TiO$_2$ nanorods. Figure 6a displays the HRTEM image of a single nanorod with a diameter of about 220 nm. The image of the nanorod tip clearly reveals that each nanorod consists of bundle of thin nanorods with approx diameter of 20 nm. The selected area electron diffraction (SAED) pattern (Fig. 6b) reveals the presence of sharp spots indicating that the samples are highly crystalline in nature. In Fig. 6c, presence of lattice fringes with interplanar spacing $d_{110} = 0.33$ nm corresponds to the rutile phase of TiO$_2$ and clearly confirms that the rods prefer to grow along (110) direction as discussed in the kinetics of growth of TiO$_2$ nanorods.

In the case of Na doped TiO$_2$ nanorods, Fig. 6d shows the HRTEM image of a single nanorod (diameter 250 nm) with the presence of sodium (as pores) on the surface of the nanorod. Each nanorod is found to comprise of individual thin nanorods with approx diameter of 25 nm. Similar to the case of undoped TiO$_2$ nanorods, the SAED pattern (Fig. 6e) reveals the presence of sharp dots indicating that the doped nanorods also possess good crystallinity. In Fig. 6f, presence of lattice fringes with interplanar spacing $d_{210} = 0.25$ nm corresponds to the rutile phase of TiO$_2$. The results are also further confirmed by EDS.

4.3 EDS analysis

The EDS spectra and chemical composition of undoped and Na doped nanorods are shown in Fig. 7a, b respectively.

Quantitative analysis of the spectrum showed that the main elements present in the undoped sample is Ti and O.
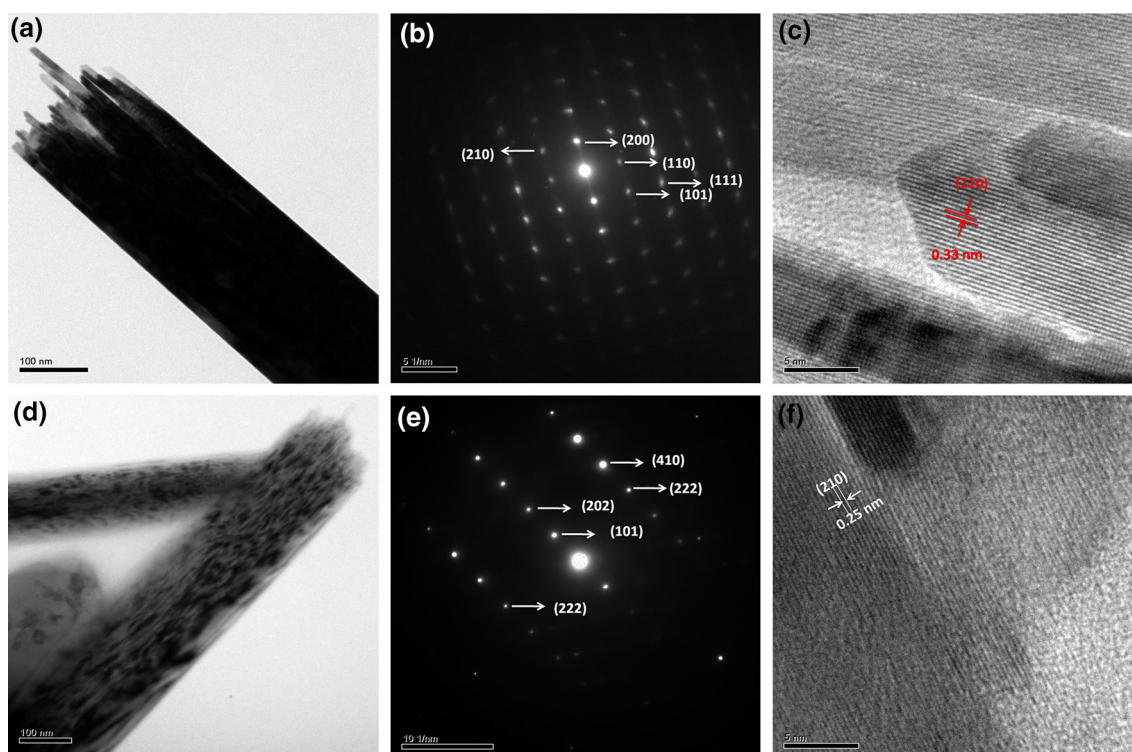
Fig. 6 HRTEM image of **a** undoped, **d** Na doped TiO$_2$ nanorods, SAED pattern of **b** undoped, **e** Na doped TiO$_2$ nanorods, Lattice fringe pattern of **c** undoped, **f** Na doped TiO$_2$ nanorods
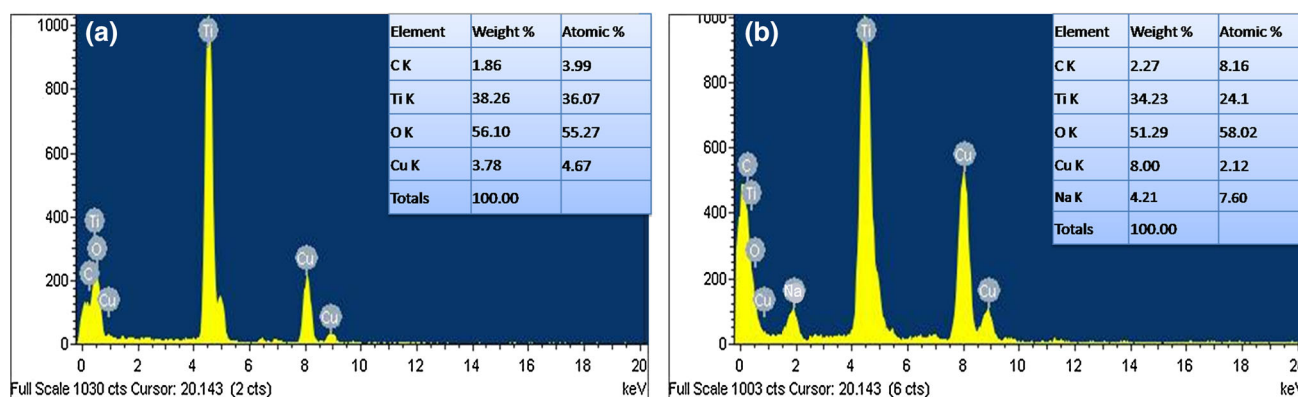

Fig. 7 EDS spectra of **a** undoped TiO$_2$ nanorods, **b** Na doped TiO$_2$ nanorods

The weight% and atomic% of the elements present is provided as inset. Peaks of copper and carbon present in the spectrum is due to the sample holder/grid used for holding the sample during analysis and the% of such elements seem to be very less. The atomic% of titanium is 36.07 and that of oxygen is 55.27 and the ratio was found to be nearly stoichiometric of 1:2. Similar to undoped samples, the main elements present in the Na doped sample is Ti, O and Na. The atomic% of titanium in this case is 24.1 and that of oxygen is 58.02 and the ratio was also found to be nearly stoichiometric of 1:2 with atomic% of Na to be 7.60 indicating the nanorods are doped with sodium.

4.4 Optical properties by UV–Vis–DRS studies

In order to study the optical properties, UV–Vis–DRS spectra of the undoped and Na doped TiO$_2$ nanorods was measured. Figure 8 shows the absorption spectra of both undoped and Na doped TiO$_2$ nanorod thin films.

As seen from the graph, all samples showed absorption with an intense transition around 420 nm in the UV region, which corresponds to the intrinsic band gap absorption of TiO$_2$. This transition is due to the electron transitions from the valence band to conduction band (O$_2$p → Ti$_3$d) of TiO$_2$ [2]. Moreover, with increase in dopant concentration, the
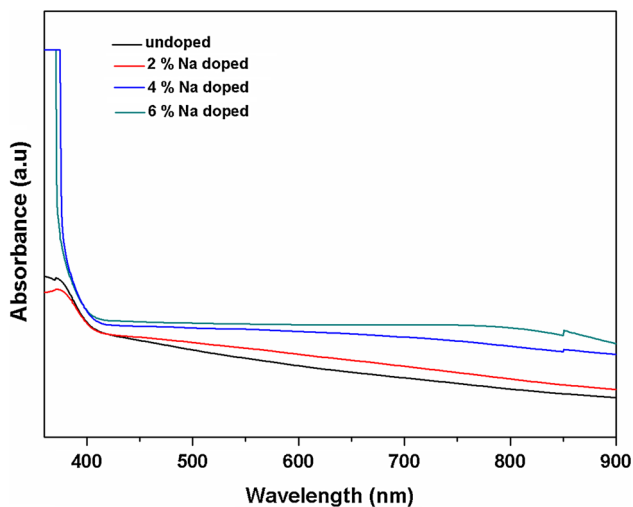
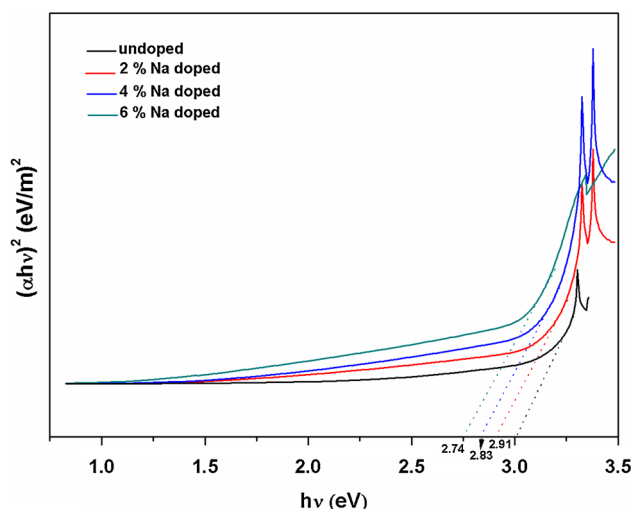**Fig. 8** Absorbance spectra of undoped, 2, 4 and 6% Na doped TiO_2 nanorod thin films

Fig. 9 Plot of $(\alpha h\nu)^2$ versus $h\nu$ for undoped, 2, 4 and 6% Na doped TiO_2 nanorod thin films

absorption edge is seen to be shifted towards the longer wavelength or towards the lesser energy side as compared to the undoped TiO_2 nanorods. The bandgap energies (E_g) of the doped samples are calculated using the equation,

$$\alpha h\nu = A(h\nu - E_g)^n \tag{1}$$

where α is the absorption coefficient, A is the absorption constant, E_g is the band gap of material, ν is the frequency of the incident radiation, h is the Planck's constant and the exponent n takes different values such as 1/2, 3/2, 2 and 3 for direct-allowed, direct-forbidden, indirect-allowed and indirect-forbidden transitions respectively [21]. In the case of TiO_2, n takes the value 1/2, considering the material exhibits direct-allowed transition.

Figure 9 shows the plot of $(\alpha h\nu)^2$ versus $h\nu$ for Na doped TiO_2 nanorod samples. From the graph, the bandgap (E_g) can be calculated by extrapolating the linear part of the curve to meet the x-axis. The E_g values as calculated from the graph is found to be respectively 2.91, 2.83 and 2.74 eV for 2, 4 and 6% Na doped TiO_2 nanorod samples compared to the E_g of 3.0 eV for undoped TiO_2 nanorod samples. From the values, it can be concluded that doping of required quantity of Na^+ into the lattice of TiO_2 can significantly reduce the bandgap values. This reduction is because, the dopant can induce the excitation of an electron from the valence band to the dope levels and form an electron-capture trap to prevent the electron–hole pairs from the process of recombination [21].

5 Conclusions

Na doped TiO_2 nanorod structures have been successfully synthesized by one-step hydrothermal method. XRD analysis of Na doped TiO_2 nanorod samples revealed the formation of single rutile phase structure. FESEM images of Na doped samples revealed the formation of nanorods and overgrowth of nanoflowers on increasing the amount of the dopant. TEM analysis revealed the formation of nanorods with a diameter about 250 nm. The presence of sodium in the nanorods was also confirmed by EDS studies. The optical studies revealed that the absorption edge shifted towards longer wavelength and the bandgap decreases from 3.0 to 2.74 eV with an increase in dopant concentration.

References

1. S. Sadhu, P. Poddar, Growth of oriented single crystalline La-doped TiO_2 nanorod arrays electrode and investigation of opto-electronic properties for enhanced photoelectrochemical activity. RSC Adv. **3**, 10363–10369 (2013)
2. X. Wu, S. Fang, Y. Zheng, J. Sun, K. Lv, Thiourea-modified TiO_2 nanorods with enhanced photocatalytic activity. Molecules **21**, 181–193 (2016)
3. A. Subramanian, H. Wen, Wang, Effects of boron doping in TiO_2 nanotubes and the performance of dye-sensitized solar cells. App. Surf. Sci. **258**, 6479–6484 (2012)
4. S. Suhaimi, M.M. Shahimin, Z.A. Alahmed, J. Chyský, A.H. Reshak, Materials for enhanced dyesensitized solar cell performance: electrochemical application. Int. J. Electrochem. Sci. **10**, 2859–2871 (2015)
5. A. Sadeghzadeh-Attar, M. Sasani Ghamsari, F. Hajiesmaeilbaigi, Sh Mirdamadi, Template-based growth of TiO_2 nanorods by sol-gel process. Semicond. Phys. Quantum Electron. **10**, 36–39 (2007)
6. S. Kathirvel, C. Su, H.-C. Lin, B.-R. Chen, W.-R. Li, Facile non-hydrolytic solvothermal synthesis of one dimensional TiO_2 nanorods for efficient dye-sensitized solar cells. Mater. Lett. **129**, 149–152 (2014)

7. B. Liu, E.S. Aydil, Growth of oriented single-crystalline rutile TiO₂ nanorods on transparent conducting substrates for dye-sensitized solar cells. J. Am. Chem. Soc. **131**, 3985–3990 (2009)

8. H. Yu, S. Zhang, H. Zhao, B. Xue, P. Liu, G. Will, High-performance TiO₂ photoanode with an efficient electron transport network for dye-sensitized solar cells. J. Phys. Chem. **113**, 16277–16282 (2009)

9. M. Mollavali, C. Falamaki, S. Rohani, Preparation of multiple-doped TiO₂ nanotube arrays with nitrogen, carbon and nickel with enhanced visible light photoelectrochemical activity via single-step anodization. Int. J. Hydrogen Energy **40**, 12239–12252 (2015)

10. H. Imahori, S. Hayashi, T. Umeyama, S. Eu, A. Oguro, S. Kang, Y. Matano, T. Shishido, S. Ngamsinlapasathian, S. Yoshikawa, Comparison of electrode structures and photovoltaic properties of porphyrin-sensitized solar cells with TiO₂ and Nb, Ge, Zr-added TiO₂ composite electrodes. Langmuir **22**, 11405–11411 (2006)

11. Y. Duan, N. Fu, Q. Liu, Y. Fang, X. Zhou, J. Zhang, Y. Lin, Sn-doped TiO₂ photoanode for dye-sensitized solar cells. J. Phys. Chem. C **113**(16), 8888–8893 (2009)

12. B. Roose, S. Pathak, U. Steiner, Doping of TiO₂ for sensitized solar cells. Chem. Soc. Rev. **44**, 8326–8349 (2015)

13. Q.P. Liu, Y. Zhou, Y.D. Duan, M. Wang, Y. Lin, Improved photovoltaic performance of dye-sensitized solar cells (DSSCs) by Zn + Mg co-doped TiO₂ electrode. Electrochim. Acta **95**, 48–53 (2013)

14. A.K. Chandiran, F. Sauvage, L. Etgar, M. Gratzel, Ga3+ and Y3+ cationic substitution in mesoporous TiO₂ photoanodes for photovoltaic applications. J. Phys. Chem. C **115**(18), 9232–9240 (2011)

15. D. Chen, D. Yang, Q. Wang, Z. Jiang, Effects of boron doping on photocatalytic activity and microstructure of titanium dioxide nanoparticles. Ind. Eng. Chem. Res. **45**(12), 4110–4116 (2006)

16. Y. Chimupala, G. Hyett, R. Simpson, R. Mitchell, R. Douthwaite, S.J. Milne, R.D. Brydson, Synthesis and characterization of mixed phase anatase TiO₂ and sodium-doped TiO₂ (B) thin films by low pressure chemical vapour deposition (LPCVD). RSC Adv. **4**, 48507–48515 (2014)

17. R. Alvarez Roca, F. Guerrero, J.A. Eiras, J.D.S. Guerra, Structural and electrical properties of Li-doped TiO₂ rutile ceramics. Ceram. Int. **41**(5), 6281–6285 (2015)

18. K. Kalyanasundaram, *Dye-Sensitized Solar Cells*, 5th edn. (EPFL Press, 2010)

19. M.B.O. Shitta, C.S. Odeyemi, A.O. Adetuyi, Photovoltaic properties of some African dyes. Mater. Sci. Res. India **5**(2), 277–282 (2008)

20. C.J. Howard, Structural thermal parameters for rutile and anatase. Acta Cryst. **B47**, 462–468 (1991)

21. W. Li, J. Yang, J. Zhang, S. Gao, Y. Luo, M. Liu, Improve photovoltaic performance of titanium dioxide nanorods based dye-sensitized solar cells by Ca-doping. Mater. Res. Bull. **57**, 177–183 (2014)

22. D.B. Shinde, S.K. Jagadale, R.K. Mane, R.M. Mane, V.B. Ghanwat, K.V. Khot, S.S. Mali, C.K. Hong, P.N. Bhosale, Time dependent facile hydrothermal synthesis of TiO₂ nanorods and their photoelectrochemical applications. Nanomed. Nanotechnol. **S7**, 1–7 (2015)

23. H. Huang, L. Pan, C. Keat Lim, H. Gong, J. Guo, M. Siu Tse, O. Kiang Tan, Hydrothermal growth of TiO₂ nanorod arrays and in situ conversion to nanotube arrays for highly efficient quantum dot-sensitized solar cells. Small (2013). doi:10.1002/smll.201203205